On the Particle Scattering Factor of Janus Micelles

3 **AUTHORS**, INCLUDING:

Tobias Futterer
Johnson & Johnson
23 PUBLICATIONS **153** CITATIONS

SEE PROFILE

Peter R Lang
Forschungszentrum Jülich
64 PUBLICATIONS **948** CITATIONS

SEE PROFILE

Particle Scattering Factor of Janus Micelles

Tobias Fütterer,[†] Gerrit A. Vliegenthart,[‡] and Peter R. Lang*,[‡]

Iwan Stranski Laboratorium, TU-Berlin, Strasse des 17 Juni 112, 10623 Berlin, Germany, and Forschungszentrum Jülich, IFF, 52425 Jülich, Germany

ABSTRACT: We calculate scattering curves from Janus micelles based on a new particle scattering factor which we tested against Monte Carlo simulations. If we compare scattering data from Janus micelles with data of core−shell particles, we find that it is virtually impossible to distinguish the particle scattering factors of the two structures, if the scattering length densities of the respective segments are similar. As intuitively expected, this situation worsens if the particles have a finite spread of radii and/or scattering length densities. We show, however, that even in this case a positive identification of Janus micelles is possible on the basis of scattering experiments, if contrast variation techniques are applied. For this purpose the outer radius of the micelle should be larger than twice the inner radius, and the scattering length densities of the two Janus face segments should differ at least by a factor of 2. The most favorable conditions occur when the scattering length density of the core is the mean value of the two outer segments.

Introduction

During the past decade polymer chemists have taken a great effort to synthesize so-called Janus micelles, a term which was coined, referring to the ancient two-faced Roman deity. Accordingly, Janus micelles are self-assembled structures, in which the surface area of the aggregate is microphase separated into two "faces". A general route to the synthesis of these structures is the use of two block copolymers A−B and A−C, which are dissolved in a medium that is a solvent for the B- and C-block but a nonsolvent for the A-block. The selectivity of the solvent will lead to the formation of micelles in the first place, in which the insoluble A-blocks are separated from the continuous medium by the soluble blocks. However, as polymers are generally chemically incompatible, it may be expected that the C- and B-blocks separate to form nanometer-scaled domains of either block.

Typically Janus particles have spherical shape,[1] although there are reports on nonspherical particles with Janus-type internal configuration.[2,3] In the present contribution we will limit the discussion to spherical particles because these are of particular interest for two reasons. First, they appear to be most easily synthesized. Second, the compartmentalization of material will as a consequence lead to symmetry break of the pair interaction potential, between two spherical particles. That is, Janus micelles are a convenient route to synthesize dipolar spheres, a type of structure which is being intensively investigated in colloidal physics.[4,5] The combination of spherical shape and nonspherosymmetric interaction potential leads to novel structures and phases not observed before.[6] Besides this fundamental aspect, it is also expected that Janus micelles may have the potential for new applications in various fields.

Experimental evidence for the internal structure of Janus particles has been gathered from a variety of techniques (see e.g. ref 1); however, a sound proof of a Janus-type compartmentalization is difficult to achieve

for various reasons. Using modern imaging techniques like SFM or STEM, the distinction between two faces of a micelle is very difficult due to lack of contrast. Structural analysis by scattering techniques is hampered by the fact that Janus particles tend to aggregate into super structures. Furthermore, there was no particle scattering function available for Janus particles until recently.[7] Even with a particle scattering factor available, it is not straightforward to identify Janus micelles in a scattering experiment because the scattering from Janus particles is merely indistinguishable from the scattering of centrosymmetric core−shell particles if the scattering contrast is not carefully selected. This is shown in Figure 2 and will be discussed in detail in the "Discussion" section.

In the present contribution we will introduce a new particle scattering factor for Janus particles which we tested against Monte Carlo calculations of the scattering function. In addition, we describe a two-step scheme of small-angle neutron scattering (SANS) data analysis which eventually allows a positive identification of Janus particles and the determination of structural parameters. The paper is organized as follows: in the section titled Particle Scattering Factor we will discuss different competing structures for Janus particles, introduce a new particle scattering factor, and relate it to the expression given by Kaya.[7] In the Discussion and Conclusions sections we will outline a two-step scheme to analyze neutron scattering data applying contrast variation. Finally, the derivation of the particle scattering factor will be given in the Appendix.
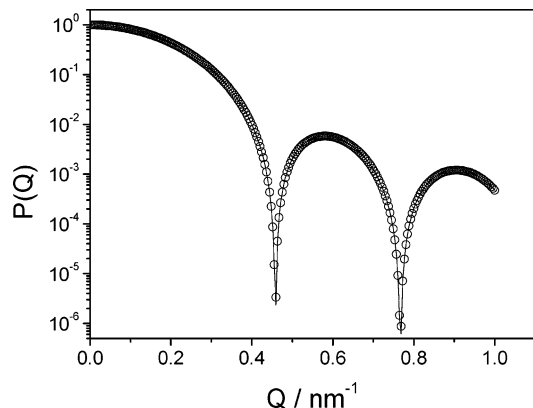
Particle Scattering Factor

If Janus micelles are synthesized from a mixture of A−B and A−C block copolymers (BCP) according to the general route sketched in the Introduction, there are three limiting structures to which the BCP may self-assemble in a medium which is a solvent for the B- and C-block and a nonsolvent for the A-block. If the B-blocks separate completely from the C-blocks and two hemispherical caps are formed, the desired configuration is obtained. As the opposite limit one might imagine a structure where the two blocks in the corona are evenly distributed. In between these two limits there could as

[†] TU-Berlin.
[‡] Forschungszentrum Jülich.
* Corresponding author: e-mail p.lang@fz-juelich.de.
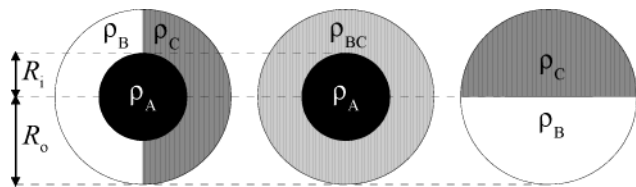
Figure 1. Sketch of competing particle structures. From left to right: Janus micelle, core—shell particle, and simplified Janus micelle.

Figure 2. Comparison of the particle scattering factors of a Janus micelle (○) and a the competing core—shell structure (—) according to eqs 1—3 and 5. The structural parameters were set to $R_o = 10$ nm, $R_i = 5$ nm, $\rho_A = 0.956$, $\rho_B = 0.819$, and $\rho_C = 0.808$ according to a Janus particle consisting of a polybutadiene core (A) and the two half-shells consisting of polystyrene (B) and poly(methyl methacrylate) (C). Here data smearing due to limited experimental resolution was not taken into account in the calculations of the form factors.

well occur intermediate structures, in which one of the blocks, say the C-block, forms a continuous background with speckles of the other block, say B. The third limiting case is the formation of two populations of micelles one consisting of AB core—shell particles and the other of AC core—shell particles. In what follows we will confine the discussion to the two structures mentioned first; i.e., we will use the term Janus particle for an entity consisting of a spherical core with the scattering length density (SLD) ρ_A and the radius R_i covered with two hemispherical caps with the respective scattering length densities ρ_B and ρ_C. The entire assembly has the radius R_o (see Figure 1, left). The term core—shell particle will be assigned to the type of particle which is sketched in the middle of Figure 1, where the SLD of the shell is constant $\rho_{BC} = (\rho_B + \rho_C)/2$ throughout the shell. The radius and the SLD of the core as well as the outer radius of the particle are the same as for the Janus particle, i.e., R_i, ρ_A, and R_o, respectively. On the right side of Figure 1 we have also sketched the simplified Janus structure for which Kaya has published the particle scattering factor,[7] i.e., two-half spheres with radius R_o divided by a plane.

The particle scattering factors or form factors for objects that do not have spherical symmetry can be generally written as

$$P(Q) = \frac{1}{4\pi} \int_0^{2\pi} \phi \int_0^{\pi} b(\mathbf{Q},\theta,\phi)^2 \sin\theta \, d\theta \tag{1}$$

where θ and ϕ are the tilt and the azimuthal angle of $\mathbf{Q}$ with respect to the Cartesian z-axis. The two integrals represent averaging of the particle orientation with respect to the scattering vector $\mathbf{Q}$. The form amplitude

$b(\mathbf{Q},\theta)$ is the normalized Fourier transform of the excess SLD distribution in the particle with respect to the solvent.

$$b(\mathbf{Q},\theta,\phi) = \frac{\int \rho(\mathbf{r}) \exp\{i\mathbf{Q}\cdot\mathbf{r}\} \, d\mathbf{r}}{\int \rho(\mathbf{r}) \, d\mathbf{r}} \tag{2}$$

The integral in the denominator of eq 2 is a normalization constant and will be called V_n in what follows. For a spherical particle with constant SLD it is the product of the sphere volume and the SLD.

For the Janus micelle (Figure 1, left), the square of the form factor amplitude is given by

$$b_J^2(\mathbf{Q},\theta) = \frac{4\pi^2}{Q^2(1-\mu^2)V_n^2}\{[(\rho_B + \rho_C) \times$$
$$\int_0^{R_o}\cos(kz)F(R_o,z,\mu)\,dz + (\Delta_{BA} + \Delta_{CA}) \times$$
$$\int_0^{R_i}\cos(kz)F(R_i,z,\mu)\,dz]^2 + ([\rho_B - \rho_C)\int_0^{R_o}\sin(kz)F \times$$
$$(R_o,z,\mu)\,dz + (\Delta_{BA} - \Delta_{CA})\int_0^{R_i}\sin(kz)F(R_i,z,\mu)\,dz]^2\} \tag{3}$$

where $Q = |\mathbf{Q}|$, $\mu = \cos\theta$, $k = Q\mu$, $\Delta_{BA} = \rho_A - \rho_B$, $\Delta_{CA} = \rho_A - \rho_C$, and the functions $F(R_j,z,\mu)$ are given by $F(R_j,z,\mu) = \sqrt{R_j^2 - z^2}J_1(Q\sqrt{1-\mu^2}\sqrt{R_j^2 - z^2})$, with J_1 the Bessel function of first order. For this structure the normalization constant is $V_n = {}^2\!/_3\pi((\rho_B + \rho_C)(R_o^3 - R_i^3) + 2\rho_A R_i^3)$. Note that the form amplitude does no longer depend on ϕ, since Janus particles have cylindrical symmetry (see Appendix).

For the two half-sphere structures (Figure 1, right) the square of the form factor amplitude reduces to the expression given by Kaya,[7] which in our notation reads

$$b_{hs}^2(\mathbf{Q},\theta) = \frac{4\pi^2}{Q^2(1-\mu^2)V_n^2}\{[(\rho_B + \rho_C) \times$$
$$\int_0^{R_o}\cos(kz)F(R_o,z,\mu)\,dz]^2 +$$
$$[(\rho_B - \rho_C)\int_0^{R_o}\sin(kz)F(R_o,z,\mu)\,dz]^2\} \tag{4}$$

In this case the normalization constant reduces to $V_n = {}^2\!/_3\pi(\rho_B + \rho_C)R_o^3$.

While the calculation of form factors using eq 3 or eq 4 has to be done numerically, the particle scattering factor of a core—shell structure (Figure 1, middle) can be written in a closed analytical form as[8,9]

$$P_{cs}(Q) = \left(\frac{4\pi}{Q^3 V_n}[(\rho_A - \rho_{BC})(\sin(QR_i) - QR_i \times$$
$$\cos(QR_i)) + \rho_{BC}(\sin(QR_o) - QR_o \cos(QR_o))]\right)^2 \tag{5}$$

where $V_n = {}^4\!/_3\pi(\rho_A R_i^3 + \rho_{BC} R_o^3)$. For a single particle the scattered intensity is related to the form factor by $I(Q) = V_n^2 P(Q)$.

In the calculation of the SANS curves presented in the next section we used normalized excess scattering length densities ρ_j (j = A, B, C) which are related to absolute values as follows:

$$\rho_j = \frac{\rho_j^{abs} - \rho_{D-solvent}^{abs}}{\rho_{H-solvent}^{abs} - \rho_{D-solvent}^{abs}}$$

for the particle segments and

$$\rho_{solvent} = \frac{\rho_{solvent}^{abs} - \rho_{D-solvent}^{abs}}{\rho_{H-solvent}^{abs} - \rho_{D-solvent}^{abs}}$$

for solvent mixtures. The superscript abs refers to absolute scattering length densities expressed in units of a squared reciprocal length. Here $\rho_{D-solvent}^{abs}$ and $\rho_{H-solvent}^{abs}$ are the absolute scattering length densities of a deuterated and a protonated solvent, respectively. We have chosen this normalization scheme, which might appear to be unusual, because it facilitates the comparison of different contrast scenarios. $\rho_{solvent}$ varies from zero (fully deuterated solvent) to unity (fully protonated solvent) and the individual segments match the protonated solvent for $\rho_j = 1$ and the deuterated solvent for $\rho_j = 0$. According to the normalization of the scattering length densities, also calculated intensities will be normalized, and they are related to absolute values by

$$I(Q) = \frac{I(Q)^{abs}}{(\rho_{H-solvent}^{abs} - \rho_{D-solvent}^{abs})^2}$$

To mimic real SANS experiments as close as possible, we took into account data smearing in the analytical calculation of the scattering curves. If not explicitly stated otherwise, the ideal model scattering functions were smeared with a wavelength distribution, an angular spread, and a finite detector resolution applying a Gaussian-type resolution function as suggested by Barker et al.[10]

In the above expression for $b(\mathbf{Q},\theta)$ it is assumed that the SLD is constant in the respective segments. Although there are reports on SANS experiments which imply a homogeneous SLD in the shell of core−shell particles,[11,12] this is very probably not generally the case. A more likely structural model has to allow for a smooth transition from the core SLD to the corona SLD and further for a decay of the number density of scattering centers in the corona with increasing distance from the particle center $r = |\mathbf{r}|$. These features however cannot be implemented easily into the analytical expression for the particle scattering factor.

Therefore, we chose to calculate the scattered intensity using Monte Carlo simulations where we considered a single spherical particle containing N scattering elements. The local number density of scattering elements at position $\mathbf{r}$ is $\eta(\mathbf{r}) = \sum_j^N \delta(\mathbf{r} - \mathbf{r}_j)$. The scattering length at this point is introduced through the weight function $w(\mathbf{r})$, and thus, the local scattering length density is $\rho(\mathbf{r}) = \eta(\mathbf{r})w(\mathbf{r})$.

The scattering intensity is given by

$$I(\mathbf{Q}) = \langle \rho(\mathbf{Q})\, \rho(-\mathbf{Q}) \rangle \qquad (6)$$

where $\rho(\mathbf{Q})$ are the Fourier components of the scattering length density defined as $\rho(\mathbf{Q}) = \int \rho(\mathbf{r}) \exp(i\mathbf{Q}\cdot\mathbf{r})\, d\mathbf{r} = \sum_j^N w(\mathbf{r}_j) \exp(i\mathbf{Q}\cdot\mathbf{r}_j)$ The form factor is defined as $P(\mathbf{Q}) = I(\mathbf{Q})/I(\mathbf{Q}{=}0)$.

In our simulations, we take η_A constant throughout the core and chose a radial decay of $\eta_{BC}(\mathbf{r})$ in the corona

segments, according to the Daoud−Cotton model for spherical brushes,[13] i.e., $\eta_{BC}(\mathbf{r}) = \eta_0/r$. Here η_0 is an amplitude defined as $\eta_0 = \eta_A R_i$ to ensure that the core and the respective corona segments have equal number densities at $r = R_i$. The radial decay is cut off at $r = R_o$. On top of this, the local SLD was adjusted by the weight function $w(\mathbf{r})$. We put the center of the sphere at the origin and take the xy-plane as the dividing plane between the two outer half-spheres. For each of the half-spheres, $w(\mathbf{r})$ is only a function of r. To model a smooth density profile from the core to the corona of the sphere, we use a tanh profile

$$w(r) = \begin{cases} \dfrac{\rho_B - \rho_A}{2} \tanh\!\left(\dfrac{r - R_i}{d}\right) + \dfrac{\rho_B + \rho_A}{2} & \text{for } r < 0 \\[3mm] \dfrac{\rho_C - \rho_A}{2} \tanh\!\left(\dfrac{r - R_i}{d}\right) + \dfrac{\rho_C + \rho_A}{2} & \text{for } r \geq 0 \end{cases}$$
$$(7)$$

This functional form gives a gradual change of the scattering density between ρ_A and ρ_B or ρ_C The parameter d sets the sharpness of the interface between core and corona. The model does not take into account a diffuse interface between the two outer half-spheres.

The actual MC calculations were performed as follows. An initial configuration was created by generating N points randomly in a sphere of unit radius. To each of these N points the appropriate weight $w(\mathbf{r})$ was attributed. Rotationally averaged intensities were determined by averaging $I(Q)$ over M configurations obtained by rotating the sphere around a randomly chosen axis over a randomly chosen angle. In the cases where analytical expressions are available, we find perfect agreement with the MC calculations for $N = 100\,000$ and $M = 100$. For the other cases we chose $N = 100\,000$ and $M = 200$, since further increasing these numbers does not change the results.

Discussion

Usually SANS data are analyzed by nonlinear least-squares fitting of the experimental data with an appropriate particle scattering factor. In Figure 2 the major problem of this procedure is illustrated. We have calculated form factors for a realistic system with the potential to form Janus micelle as it was synthesized by Erhardt et al.[1] According to there synthesis, it is highly probable that the particles have a Janus-type structure with a polybutadiene core (A) and two-half shells which consist of polystyrene blocks (B) and poly-(methyl methacrylate) blocks (C), where all three blocks were fully protonated. On the basis of the bulk densities of the three polymers and the deuterated solvent tetrahydrofuran, the scattering length densities can be estimated to be $\rho_A = 0.956$, $\rho_B = 0.819$, and $\rho_C = 0.808$. In the competing core−shell structure in which the B- and C-blocks do not separate, the SLD of the shell is $\rho_{BC} = 0.813$. Using these SLDs, we calculated the particle scattering factors of a Janus micelle and of the core−shell particle which are shown in Figure 2. Here we did not take into account data smearing; nevertheless, the curves are virtually identical. Even worse, in a real experiment tiny differences, if there were any, would be smeared due to the limited experimental resolution. It is thus obvious that a Janus micelle cannot be distinguished from a core−shell particle by one single scattering experiment, but elaborate contrast variation experiments have to be applied.
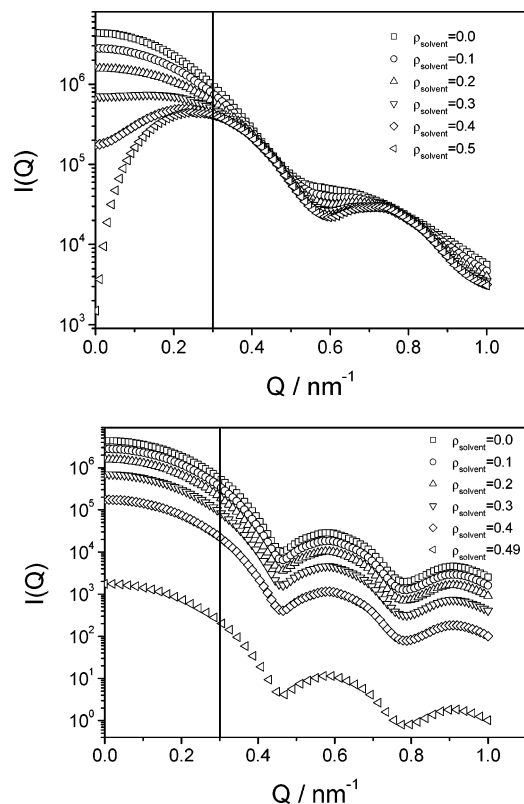
Figure 3. Top: scattered intensity curves for a Janus particle with $R_o = 10$ nm, $R_i = 5$ nm, $\rho_A = 0.5$, $\rho_B = 1.0$, and $\rho_C = 0.0$. Bottom: scattered intensity curves for the competing "core–shell" structure with $R_o = 10$ nm, $R_i = 5$ nm, $\rho_A = 0.5$, and $\rho_{BC} = 0.5$. The solvent scattering length density varies as indicated in the legend. The vertical lines at $Q_f = 0.3$ nm^{-1} represent the cuts along which the absolute intensities at fixed scattering vector were calculated that are plotted in Figure 4.

This can be done rather easily in SANS because it is very easy to change the scattering contrast, i.e., the excess SLD of certain particle segments by mixing deuterated and protonated solvent. As a consequence, the absolute scattering intensity $I(Q) = V_n^2 P(Q)$ at a given scattering vector will change. For particles with segments of different excess scattering length densities the Q dependence of $P(Q)$ changes as well. This is illustrated in Figure 3, where we have collected scattering curves, $I(Q)$ vs Q, of Janus micelles and core–shell particles at different contrasts.

These curves were calculated for an idealized contrast situation which will be discussed later. However, they show that by contrast variation it is well possible to distinguish between the competing structures. Consequently, SANS experiments should be performed at a series of solvent SLD, and the intensity data should be analyzed in a simultaneous nonlinear least-squares fit of eqs 1–3 to the data. However, the required numerical integrations would cause this strategy to be computationally very time-consuming—even more so if experimental data smearing has to be taken into account. Therefore, we suggest a procedure that allows to decide beforehand whether the particles have a Janus-type or core–shell configuration.

To distinguish between the two competing structures, the most feasible contrast situation is $\rho_B = 1$, $\rho_C = 0$, and $\rho_A = 0.5$; i.e., the SLD of one half-shell matches $\rho_{H-solvent}^{abs}$ and that of the other matches $\rho_{D-solvent}^{abs}$. In this situation the particle scatters as a sphere with constant SLD, if the corona blocks mix completely. That is the
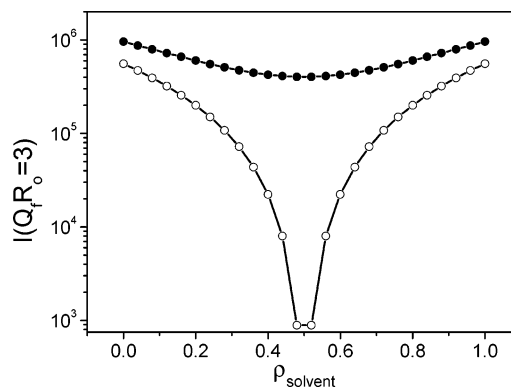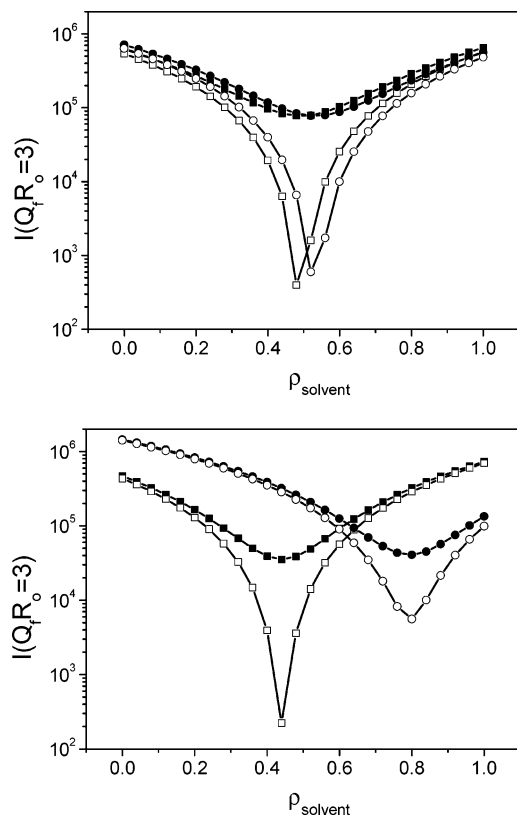

Figure 4. Scattered intensity at fixed $Q_f R_o = 3$ for a Janus particle (full circles) with $R_o = 10$ nm, $R_i = 5$ nm, $\rho_A = 0.5$, $\rho_B = 1.0$, and $\rho_C = 0.0$ and for the competing core–shell (open circles) structure with $R_o = 10$ nm, $R_i = 5$ nm, $\rho_A = 0.5$, and $\rho_{BC} = 0.5$.

angular dependence of $P(Q)$ does not change with the solvent SLD, and the absolute intensity scales as V_n^2 at any scattering vector. For such a core–shell particle it is possible to match the solvent SLD to the particle. In this case the scattered intensity becomes zero throughout the entire Q range because $V_n^2 \rightarrow 0$. For the competing Janus particle the situation is fundamentally different in two respects. (i) V_n^2 cannot become zero except for the unphysical case of $R_o = 0$. (ii) The shape of the particle scattering factor $P(Q)$ varies with the SLD of the solvent. For example, position and relative depth of the form factor minima change with scattering contrast, as is shown in Figure 3.

These two differences set the stage for a procedure to distinguish between a Janus micelle and the competing core–shell particle. According to point (i) the scattered intensity at a fixed scattering vector from a core–shell particle $I_{CS}(Q_f)$ runs though a distinct minimum, if the solvent SLD is varied in the range $0 \leq \rho_{solvent} \leq 1$, as is shown in Figure 4, where $I_{CS}(Q_f)$ vs $\rho_{solvent}$ at $Q_f R_o = 3$ is plotted according to the vertical cuts indicated in Figure 3. The corresponding curve for the Janus particle is shown as well. Extensive testing of numerous scattering curves showed that a range of $3 < Q_f R_o < 4$ is most suitable for this kind of data analysis.

The scattered intensity at Q_f from the Janus particle varies less than a factor of 10 while the intensity scattered from the competing core–shell structure spans a region of 3 orders of magnitude as the solvent SLD changes from purely protonated to purely deuterated solvent. This may be regarded as a fingerprint of the core–shell structure in contrast to the Janus micelle.

It is probably very difficult, if not impossible, to set the SLDs of the respective particle segments by chemical synthesis exactly as we assumed in the above calculation. Therefore, we tested whether similarly significant differences are observed for different contrast scenarios and different ratios of the radii. Generally we found that a spread of radii and/or SLD distributions smears out the dip in the $I(Q_f R_o=3)$ vs $\rho_{solvent}$ curves of core–shell particles as compared to the curve displayed in Figure 4. Nevertheless, the difference in absolute scattered intensity between the Janus micelle and the core–shell particle appears to be a very robust criterion for the distinction between the two competing structures. This is due to the fact that in the case of a core–shell particle there is always a ratio of SLDs which allows for an average matching to the solvent SLD.
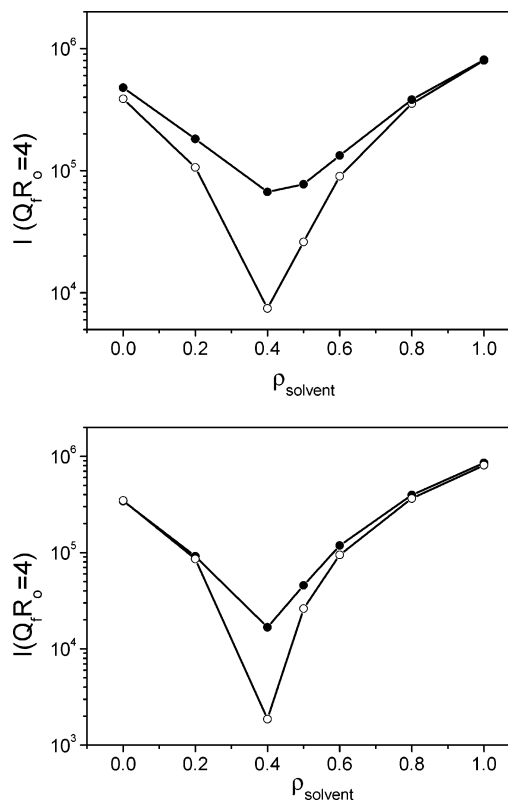
Figure 5. Scattered intensity at fixed $Q_f R_o = 3$ for Janus particles (full symbols) and competing core−shell structures (open symbols) with $R_o = 10$ nm, $R_i = 3$ nm (top), and $R_i = 7$ nm (bottom). The scattering length densities in the corona region were set to $\rho_B = 0.7$ and $\rho_C = 0.3$ with $\rho_{BC} = (\rho_C + \rho_B)/2$. For the core we chose $\rho_A = 0.4$ (squares) and $\rho_A = 1.0$ (circles).

From the matching condition $V_n = 0$ this ratio is easily calculated to be $\rho_A/\rho_{BC} = -R_o^3/R_i^3$. On the other hand, average matching of the particle's SLD to the solvent is not possible in the case of the Janus structure. In this case the matching condition can only be met if $\rho_B = \rho_C$, which again corresponds to a core−shell particle. Further examples for the intensity variation with solvent SLD are shown in Figure 5 for four different scenarios.

Generally the curves show only minor changes with the ratio of the radii or the relative SLDs of the segments as long as either $\rho_B \le \rho_A \le \rho_C$ or $R_i < R_o/2$. The difference between the competing structures is the least if the core radius approaches the outer particle radius and if the core has the highest SLD of the three particle segments. In this sense the variation of the absolute scattered intensity at an appropriately chosen Q_f with solvent SLD may be regarded as a sound criterion to distinguish between a Janus-type particle and the competing core−shell structure.

Actually it even holds for systems where the change of SLD between core and corona segments is smeared and the SLD of the shell segments varies with the distance to the center as one should expect for real particles. Using the Monte Carlo scheme described in the section Particle Scattering Factor, we have simulated scattering curves for a system where the scattering length density of the core is $\rho_A = 0.4$, and in the corona segmets the SLDs are $\rho_B = 0.7$ and $\rho_C = 0.3$ with $\rho_{BC} = (\rho_C + \rho_B)/2$. According to eq 7, we chose a tanh function for the continuous transition from the core to the respective corona density. Further we superimposed a radial distribution of the SLD in the shell segments

Figure 6. Results of the Monte Carlo calculations for the scattered intensity at fixed $Q_f R_o = 4$ for Janus particles (full symbols) and competing core−shell structures (open symbols) with $R_o = 10$ nm, $R_i = 3$ nm (top), and $R_i = 7$ nm (bottom). The scattering length densities in the corona region were set to $\rho_B = 0.7$ and $\rho_C = 0.3$ with $\rho_{BC} = (\rho_C + \rho_B)/2$. For the core we chose $\rho_A = 0.4$. In the corona segments the number density of scatterers decays as $1/r$, and a continuous density change from the core to the outer particle segment was simulated applying a tanh function with a width of $d = 0.05R_i$ according to eq 7.

according to the Daoud−Cotton[13] model. We simulated data for two different ratios of radii, i.e., $R_i/R_o = 0.3$ and 0.7. The width of the transition zone is $d = 0.05R_o$ in both cases. In Figure 6, the scattered intensities at fixed scattering vector are plotted as $I(Q_f R_o=4)$ vs $\rho_{solvent}$ together with the corresponding curve for the Janus micelle.

It is evident from the top part of Figure 6 that even for particles with a continuous transition from the core SLD to the corona SLD and a radial distribution of the corona SLD the scattered intensity of the Janus particle varies less than a factor of 10 with the solvent SLD at fixed $Q_f R_o = 4$, while the scattered intensity from the competing core−shell structure has a significant dip with a depth of more than 2 orders of magnitude, if R_o is at least twice as large as R_i. However, this effect is drastically reduced if the radius of the core exceeds roughly half of the outer radius, as is to be seen from the bottom part of Figure 6. If $R_i/R_o = 0.7$, the depth of the minimum in the intensity vs solvent SLD curve is still about 2 orders of magnitude for the core−shell structure. However, in the case of the Janus structure the intensity also varies by a factor of about 50.

On the basis of this consideration one may conclude that Janus particles are likely to be present, if the variation of the scattered intensity at $3 < Q_f R_o < 4$ is less than 2 orders of magnitude, when the solvent SLD changes from zero to one. In this case the structural

parameters of the Janus micelle may be obtained by a simultaneous fit of eqs 1–3 to experimental scattering curves recorded at a sufficiently high number of different solvent SLD.

Conclusion

We have shown that the distinction between a Janus-type particle structure and a competing core–shell particle with SANS requires elaborate contrast variation techniques. On the basis of model calculations with a new particle scattering factor for the Janus structure and simulated scattering data, we suggest a two-step procedure to identify and characterize Janus micelles. In the first step the variation of the scattered intensity at a fixed scattering vector $3 < Q_f R_0 < 4$ with the solvent SLD should be analyzed. If $I(Q_f)$ varies less than about 2 orders of magnitude while $\rho_{solvent}$ is tuned from zero to one, this may be regarded as strong evidence for the presence of Janus micelles. Only then it is worthwhile to take the remarkable computational effort of the second step, that is, a simultaneous least-squares fitting of the $I(Q)$ vs Q data recorded at various contrasts with the model form factor given by eqs 1–3. As Kaya has already pointed out, it is of large importance that the three segments have a strong tendency to segregation; otherwise, the typical features of the scattering curves will be smeared out and eventually make a thorough analysis of the data impossible. Further the distinction between the two competing structures is facilitated if, as a rule of thumb, the outer radius is larger than twice the core radius and if the ratio of the SLDs for the two half-shells is as large as possible, typically $\rho_B/\rho_C > 2$. The most suitable contrast situation would occur if the core density is $\rho_A = (\rho_B + \rho_C)/2$, which is certainly a challenge for the synthesist.

Acknowledgment. We thank G. Nägele for helpful discussions.

Appendix

The form amplitude of a particle of arbitrary shape is defined as the normalized three-dimensional Fourier transform of the particles scattering length density distribution $\rho(\mathbf{r})$. In Carthesian coordinates this is

$$b(\mathbf{Q},\theta,\phi) = \frac{1}{V_n}\int \rho(\mathbf{r})\,\exp(i\mathbf{Q}\cdot\mathbf{r})\,d\mathbf{r} \qquad (A1)$$

where the normalization constant in the denominator is the integrated scattering length density $V_n = \int \rho(\mathbf{r})\,d\mathbf{r}$ and θ is the angle between the scattering vector $\mathbf{Q}$ and the z-axis.

Although we are considering particles with spherical geometry, Janus micelles have cylindrical symmetry. It is therefore most convenient to perform the calculations in cylindrical coordinates as they are defined in Figure 7. If the scattering vector is placed in the xz-plane, its y-component is zero. Thus, the scattering vector, the positional vector, and their inner product are

$$\mathbf{Q} = \begin{pmatrix} \sin\theta \\ 0 \\ \cos\theta \end{pmatrix}; \quad \mathbf{r} = \begin{pmatrix} r_c \cos\varphi \\ r_c \sin\varphi \\ z \end{pmatrix}$$

$$\mathbf{Q}\cdot\mathbf{r} = Q(r_c\sqrt{1-\mu^2}\cos\varphi + \mu z) \qquad (A2)$$
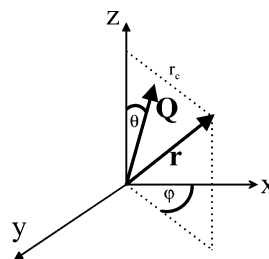
Figure 7. For the definition of the cylindrical coordinates used in the calculations. The scattering vector is placed in the xz-plane.

respectively, where $\mu = \cos\theta$ and the volume element is $d\mathbf{r} = dr_c(r_c d\varphi)\,dz$.

We now calculate first the form factor of a simple Janus particle, which consists of two half-spheres with radius R_0, each of which has a homogeneous scattering length density

$$\rho(\mathbf{r}) = \rho_C \quad \text{for } 0 \le \delta < \pi \text{ and } |\mathbf{r}| \le R_0$$

$$\rho(\mathbf{r}) = \rho_B \quad \text{for } \pi \le \delta < 2\pi \text{ and } |\mathbf{r}| \le R_0$$

where δ is the tilt angle between $\mathbf{r}$ and the plane dividing the two half-spheres. The form amplitude is then

$$b_{hs}(\mathbf{Q},\mu) = \frac{1}{V_n}[\rho_B\int_{-R_0}^{0}\exp(iQ\mu z)\,dz + $$
$$\rho_C\int_{0}^{R_0}\exp(iQ\mu z)\,dz] \times$$
$$\int_{0}^{r_{c,max}} r_c\,dr_c\int_{0}^{2\pi}\exp(iQr_c\sqrt{1-\mu^2}\cos\varphi)\,d\varphi \quad (A3)$$

The integral over φ is an integral representation of a Bessel function of zero order $J_0(x) = \int_0^{2\pi}\exp(ix\cos\alpha)\,d\alpha/2\pi$. For the second integration it has to be taken into account that the upper limit of r_c is not simply R_0 but it depends on z, i.e., $r_{c,max} = \sqrt{R_0^2 - z^2}$. If we substitute $Qr_c\sqrt{1-\mu^2} \equiv x$ and $dx = Q\sqrt{1-\mu^2}\,dr_c$, the upper integration limit over r_c becomes $u = Q\sqrt{1-\mu^2}\sqrt{R_0^2 - z^2}$, and the integral may be rewritten as $\sqrt{R_0^2 - z^2}J_1(u)/Q\sqrt{1-\mu^2}$, where we made use of the general property of Bessel functions $\int_0^A xJ_0(x)\,dx = AJ_1(A)$. Now the form amplitude becomes

$$b_{hs}(\mathbf{Q},\mu) = \frac{2\pi}{V_n Q\sqrt{1-\mu^2}}[\rho_B\int_{-R_0}^{0}\sqrt{R_0^2 - z^2}J_1(u)\times$$
$$\exp\{iQ\mu z\}\,dz + \rho_C\int_{0}^{R_0}\sqrt{R_0^2 - z^2}J_1(u)\exp\{iQ\mu z\}\,dz] \qquad (A4)$$

and the absolute square $b_{hs}^2(\mathbf{Q},\mu) = b(\mathbf{Q},\mu)b^*(\mathbf{Q},\mu)$ is

$$b_{hs}^2(\mathbf{Q},\mu) = \frac{4\pi^2}{Q^2 V_n^2(1-\mu^2)}[((\rho_B + \rho_C)\times$$
$$\int_{0}^{R_0}\cos(Q\mu z)\sqrt{R_0^2 - z^2}J_1(u)\,dz)^2 +$$
$$((\rho_B - \rho_C)\int_{0}^{R_0}\sin(Q\mu z)\sqrt{R_0^2 - z^2}J_1(u)\,dz)^2] \qquad (A5)$$

The form amplitude of a Janus particle consisting of a core with scattering length density ρ_A and radius R_i covered with two semispherical caps of radius R_0 and scattering length densities ρ_B and ρ_C, respectively, can

be derived from eq A4 by replacing a spherical portion in the center of the simple structure by a sphere with ρ_A and R_i, which yields

$$b_J(\mathbf{Q},\mu) = \frac{2\pi}{QV_n\sqrt{1-\mu^2}}[\rho_B\int_{-R_o}^0\sqrt{{R_o}^2 - z^2}J_1(u_o) \times$$

$$\exp\{iQ\mu z\}\,dz + (\rho_A - \rho_B)\int_{-R_i}^0\sqrt{{R_i}^2 - z^2}J_1(u_i) \times$$

$$\exp\{iQ\mu z\}\,dz + \rho_C\int_0^{R_o}\sqrt{{R_o}^2 - z^2}J_1(u_o) \times$$

$$\exp\{iQ\mu z\}\,dz + (\rho_A - \rho_C)\int_0^{R_i}\sqrt{{R_i}^2 - z^2}J_1(u_i) \times$$

$$\exp\{iQ\mu z\}\,dz] \quad (A6)$$

It is, though rather tedious, straightforward to calculate the absolute square $b_J^2(\mathbf{Q},\mu)$ which is given in eq 3 of the main text.

References and Notes

(1) Erhardt, R.; Zhang, M.; Böker, A.; Zettl, H.; Abetz, C.; Frederik, P.; Krausch, G.; Abetz, V.; Müller, A. H. E. *J. Am. Chem. So*c. **2003**, *125*, 3260. Erhardt, R.; Böker, A.; Zettl, H.; Kaya, H.; Pyckhout-Hintzen, W.; Krausch, G.; Abetz, V.; Müller, A. H. E. *Macromolecules* **2001**, *43*, 1069 and references given therein.

(2) Bo, Z.; Rabe, J. P.; Schlüter, A. *Angew. Chem.* **1999**, *111*, 2540.

(3) Heroguez, V.; Gnanou, Y.; Fontanille, M. *Macromolecules* **1997**, *30*, 4791.

(4) Lindlar, B.; Boldt, M.; Eiden-Assmann, S.; Maret, G. *Adv. Mater.* **2002**, *14*, 1656.

(5) Koenderink, G. H. Rotational and Translational Diffusion in Colloidal Mixtures. Ph.D. Thesis, Universiteit Utrecht, The Netherlands, 2003.

(6) Erdmann, T.; Kröger, M.; Hess, S. *Phys. Rev. E* **2003**, *67*, 041209.

(7) Kaya, H. *Appl. Phys. A* **2002**, *74*, 507.

(8) Livsey, I.; Ottewill, R. H. *Adv. Colloid Interface Sci.* **1991**, *36*, 173.

(9) Kerker, M.; Kratohvil, J. P.; Matijevic, E. *J. Opt. Soc. Am.* **1962**, *52*, 551.

(10) Barker, J. G.; Pedersen, J. S. *J. Appl. Crystallogr.* **1995**, *28*, 105.

(11) Gohr, K.; Schärtl, W.; Willner, L.; Pyckhout-Hintzen, W. *Macromolecules* **2002**, *35*, 9110.

(12) Stellbrink, J.; Rother, G.; Laurati, M.; Lund, R.; Willner, L.; Richter, D. *J. Phys.: Condens. Matter,* in press.

(13) Daoud, M.; Cotton, J. P. *J. Phys. (Paris)* **1982**, *43*, 531.